THE JOURNAL OF PHYSICAL CHEMISTRY C

Article

Cite This: J. Phys. Chem. C 2019, 123, 28816−28827

pubs.acs.org/JPCC

Water Trapping Dynamics in Carbohydrate-Populated Smectite Interlayer Nanopores

Sabrina E. Kelch,[†] Eric Ferrage,[‡] Bruno Lanson,[§] Laurent Charlet,[§] and Ludmilla Aristilde*[,†,∥,⊥]

[†]Soil and Crop Sciences Section, School of Integrative Plant Science, College of Agriculture and Life Sciences, Cornell University, Ithaca, New York 14853, United States

[‡]Institut de Chimie des Milieux et Matériaux de Poitiers (IC2MP), CNRS-Université de Poitiers, 86073 Poitiers, France

[§]Univ. Grenoble Alpes, Univ. Savoie Mont Blanc, CNRS, IRD, IFSTTAR, ISTerre, F-38000 Grenoble, France

[∥]Department of Biological and Environmental Engineering, College of Agriculture and Life Sciences, Cornell University, Ithaca, New York 14853, United States

[⊥]Department of Civil and Environmental Engineering, McCormick School of Engineering and Applied Science, Northwestern University, Evanston, Illinois 60208, United States

Supporting Information

ABSTRACT: Smectite-type clays play a critical role in the trapping of fluids within soil and atmospheric nanoparticles. The hydrodynamics of cation-saturated smectite nanopores are well documented. However, little is known about the influence of small organic compounds. Here we investigate the effects of carbohydrates (glucose and cellobiose), representing an important class of organic compounds, on the hydration and nanopore structures of montmorillonite, a prototypical smectite. To achieve the same amount of adsorbed water, higher relative humidity was required in the presence of the adsorbed carbohydrates than with the clay alone. The decrease in the characteristic micropore water adsorption with the clay−carbohydrate aggregates implied that water adsorption was constrained within the clay nanopore regions. The presence of carbohydrates promoted water retention as a function of gradual decrease in moisture content. Moisture-dependent X-ray diffraction patterns determined that, relative to the mineral alone, greater nanopore sizes were preserved in the presence of the carbohydrates, despite severe dehydration that is expected to induce clay nanopore collapse. Fourier-transform infrared spectroscopy captured disruption in the population of exchangeable waters within the carbohydrate-populated clay nanopores, with some agreement with the measured water-desorption profiling. These new findings demonstrate that carbohydrates can restructure smectite interlayer nanopores and water trapping dynamics.

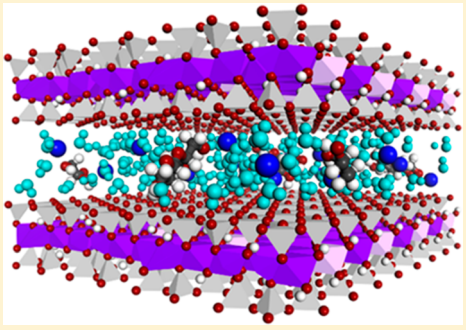

1. INTRODUCTION

Smectite clays, which are widely found in temperate-zone agricultural soils,[1,2] are also present in atmospheric mineral particles,[3−7] exploited in industrial applications and nanomaterial designs,[8−15] and recently detected in Martian soils.[16−19] Due to isomorphic substitutions in their structures, smectites have high cation exchange capacity, ranging from 0.2 to 0.6 per half unit cell.[20] The dynamics of cations and water molecules in the interlayer nanopores of cation-saturated smectites have been extensively studied.[21−26] However, little is known about the hydration behavior of smectite interlayer nanopores populated with organic compounds. Organic compounds in microbial and plant root exudates or derived from organic matter decomposition have long been implicated in enhancing soil porosity, soil moisture retention, and nutrient uptake.[27−34] Within the context of the critical role of organo-mineral nanoaggregates in facilitating long-term storage of soil moisture,[35] the objective of the present study was to investigate the influence of low-molecular-weight carbohydrates on the hydrated nanopore structure of montmorillonite (MONT), a prototypical smectite clay widely used in clay mineral studies.[22,24,36−41]

Total organics in soil solutions, which can typically range from about 0.1 to 50 μM, can reach up to 10 mM in densely rooted areas or areas with high microbial activity.[42−47] Total soil carbohydrate content has been estimated to be between 7.8 and 45 mg per g of soil,[48] and soil glucose content was found to range from 0.4 to 1.8 mg per g of soil;[49] approximately 54 μM glucose was measured in a soil solution from temperate agricultural land.[50] Therefore, carbohydrates including glucose represent an important component of the organic content in soils. Previous accurate quantitation of the adsorption of glucose and other carbohydrates on MONT[28,51,52] has been challenging due to analytical limitations whereby the commonly used dichromate−sulfuric acid method used to quantify the adsorptive concentration

Received: September 30, 2019
Revised: November 2, 2019
Published: November 4, 2019

DOI: 10.1021/acs.jpcc.9b09246
J. Phys. Chem. C 2019, 123, 28816−28827

could exhibit up to 26% error in reported data.[53] Current accurate methods for quantification of carbohydrates include mass spectrometry and combustion analysis.[54,55] Carbohydrates and other organic compounds have long been thought to impact soil water holding capacity.[56−59] Recently, Carminati et al.[60] found that the organic-rich soil near a plant rhizosphere had nearly 2-fold greater water content than the bulk soil over a range of hydration conditions. Much still remains unknown about the influence of adsorbed organic compounds including carbohydrates on the hydrated interlayer nanopores of smectite-type clays.

In hydrated cation-saturated smectite interlayers, the organization of a discrete number of water planes is typically captured by layer-to-layer distances, or d_{001}, determined from X-ray diffraction (XRD) patterns.[22,23,39,61] Specific d_{001} values have been attributed to the interlayer size of the majority of nanopores in MONT at distinct hydrated conditions: less than 1 nm for dehydrated interlayers; 1.18−1.29 nm for monohydrated (1W) interlayers; 1.45−1.58 nm for bihydrated (or 2W) interlayers; 1.80−1.95 nm for trihydrated (or 3W) interlayers.[39,61] Modeling of XRD patterns can determine quantitatively the distribution of the nanopores within the mineral matrix by taking into account the intensity, symmetry, and breadth of the experimental XRD peaks.[39,62] This symmetry and breadth of an XRD profile peak is captured by the full-width half-maximum (fwhm) metric, which is also influenced by the hydration state and structure factor. For example, totally bihydrated mineral pores will have a more intense peak (i.e., a greater intensity along the *y*-scale and less breadth) than that of completely monohydrated mineral interlayers. Generally, in hydrated MONT systems, a decrease in peak symmetry or increase in peak broadening is a function of a decrease in the homogeneity of the nanopore sizes within the mineral. Previous isotherms[63,64,37] of water adsorption on MONT have been typically described by three types of water uptake behavior as a function of relative humidity (RH) condition or moisture content. Between 20 and 50% RH, water adsorption was found to be dominated by monohydrated interlayer nanopores,[63,65] between 50 and 80% RH, the majority of interlayers became bihydrated,[37,65] and above 80% RH, trihydrated nanopores and capillary water adsorption within the structural micropore network of MONT was prevalent.[64,65] This overall water uptake behavior correlated with the trimodal water adsorption pattern of MONT, which finishes with a third exponential rate increase section from 80 to 100% RH.[63] Recently, a more detailed model was published with five adsorbed water types, which taking into account condensation and interlayer filling, highlighted five adsorbed water types.[66] Recent qualitative comparisons of XRD patterns of MONT in the presence and absence of glucose have revealed that the expected collapse of MONT interlayer nanopores in response to dehydration was diminished as a function of increasing glucose concentration.[67] The population of organics thus complicates the traditional method of determining hydration states from the interlayer nanopore sizes. Therefore, to determine the hydration state of the MONT−glucose nanoaggregates, explicit monitoring of water content within the sample would be required.

Adsorption−desorption isotherms on a microbalance or pressurized apparatus are typically used to quantify directly the amount of water present within the mineral matrix.[3,37,63,68,69] Water adsorption and desorption patterns or isotherms have been shown to differ depending on ion presence and concentration.[37,65,68] Smectite clays exhibit hydration hysteresis, characterized by a different profile of water adsorption versus water desorption.[68,69] A water adsorption isotherm study[52] of a smectite in the presence of polyethylene glycol, a polar organic polymer, found a decrease in the amount of adsorbed water as a function of an increase in the adsorbed amount of polyethylene glycol. No water desorption isotherms were performed with the polyethylene glycol−MONT composites to investigate fully the water dynamics.

Exchangeable waters, which consist primarily of free waters involved in water−water interactions or in the hydration sphere of the interlayer cations that are not closely associated with the mineral surface, have been investigated in cation-saturated MONT using attenuated total reflectance Fourier-transform infrared (ATR-FTIR) spectra[68] by monitoring the water O−H stretching bands at 3390 cm^{-1}.[3,63,68,70−72] In agreement with theoretical predictions of water organization within the MONT interlayers, FTIR data have captured an increase in the exchangeable water band as a function of increasing moisture content.[3,63,68,73] Here, in addition to cation hydration sphere and free water populations, carbohydrate-associated waters, which are expected to hydrate the carbohydrate compounds via hydrogen bonding interactions, would be included in the population of exchangeable waters, while excluding any waters that are in close proximity to the mineral surface (i.e., mineral-bound waters). No spectroscopic investigation is available regarding the influence of carbohydrates or other organic compounds on the exchangeable water dynamics within the MONT interlayer nanopores.

Here, we investigate water retention profiling, nanopore size distribution, and water dynamics in MONT populated with two relevant carbohydrate compounds: cellobiose (a disaccharide), which is a major byproduct of the microbial breakdown of cellulose, and glucose (a monosaccharide), which is a common carbohydrate in soils and an important bioavailable substrate for soil microorganisms[54,74,75] (Figure 1). We hypothesize that (1) water retention within MONT−carbohydrate aggregates will result in expanded nanopore size during dehydration and (2) water trapping will be promoted within MONT−carbohydrate aggregates due to association

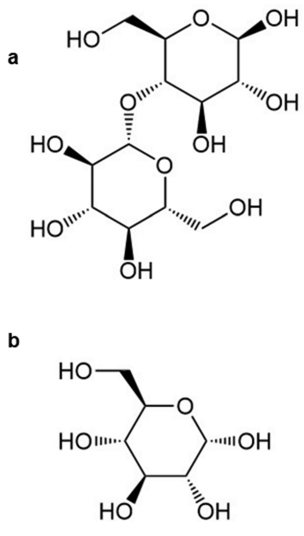

Figure 1. Chemical structures of the carbohydrates reacted with montmorillonite in this study: (a) cellobiose and (b) glucose.

DOI: 10.1021/acs.jpcc.9b09246
J. Phys. Chem. C 2019, 123, 28816−28827

with the carbohydrates and/or immobilization on the mineral surface.

To overcome the previous analytical challenges of monitoring carbohydrate adsorption on MONT, we employed combustion analysis coupled with isotope-ratio mass spectrometry (CA-IRMS). The influence of adsorbed carbohydrates on water retention within MONT aggregates was investigated by performing water adsorption−desorption isotherms. Through quantitative analysis of the XRD patterns of carbohydrate-containing MONT samples during *in situ* dehydration, we determined the moisture-dependent abundance of MONT nanopore sizes in the absence and presence of adsorbed carbohydrates. Using ATR-FTIR, we monitored the dynamics of exchangeable waters as a function of carbohydrate loading and hydration conditions. The findings presented here provide new insights into how the presence of carbohydrates and related organic compounds could influence the hydration behavior of smectite nanoaggregates, with important implications for understanding moisture retention by smectite clays within soil and atmospheric particles.

2. MATERIALS AND METHODS

2.1. Materials. Unless otherwise noted, all chemicals used were purchased from Fisher Scientific (Pittsburgh, PA, U.S.A) or Sigma-Aldrich (St. Louis, MO, U.S.A). The (UL-$^{13}C_{12}$)-cellobiose was purchased from Omicron Biochemicals (South Bend, IN, U.S.A.) and the (U−$^{13}C_6$)-glucose was purchased from Cambridge Isotope Laboratories (Andover, MA, U.S.A). The smectite clay mineral, Wyoming Na-MONT (SWy-2), was obtained from the clay repository of the Clay Mineral Society[76] (West Lafayette, IN, U.S.A.) and used as received. The structural formula of the purchased MONT[76] was reported as $(Ca_{0.12}Na_{0.32}K_{0.05})(Al_{3.01}Fe(III)_{0.41}Mn_{0.01}Mg_{0.54}Ti_{0.02})(Si_{7.98}Al_{0.02})O_{20}(OH)_4$, with an octahedral sheet charge of −0.53 and a tetrahedral sheet charge of −0.02.

2.2. Adsorption Experiments and Isotopic Carbon Analysis. Adsorption experiments were conducted by reacting 0.45 g of MONT with 30 mL of solution of each carbohydrate (cellobiose or glucose) in a 50 mL polypropylene tube with a conical bottom. Stock carbohydrate solutions were used to prepare initial cellobiose or glucose concentrations at carbon-equivalent concentrations, from 0.3 to 120 mM C. Solutions were made in a 0.1 M NaCl background solution with 0.02 M $NaHCO_3$ as a buffer, adjusted to pH 6.5 with small aliquots of 1 M HCl. Control experiments, in the absence of the carbohydrates, were conducted with MONT in the same background solution. Unless otherwise noted, samples were shaken for 240 h before removing the supernatant.

To quantify the amount of carbohydrate-carbon adsorbed on MONT during the adsorption experiments, ^{13}C-labeled carbohydrates were used. Specifically, MONT was reacted with three different initial carbon-equivalent concentrations of glucose (0.1, 2, and 20 mM with respectively 100%, 100%, and 1% $^{13}C_6$-glucose or cellobiose (0.05, 1, and 10 mM with respectively 50%, 5%, and 1% $^{13}C_{12}$-cellobiose. Samples were taken at kinetic time points (0, 12, 24, 60, 90, 180, and 240 h). Tubes were prepared in triplicate for each concentration of cellobiose or glucose for each kinetic time point. After centrifugation, the samples were freeze-dried for 24 h and ground to homogeneity before being analyzed on a combustion elemental analyzer connected to a ThermoScientific isotope ratio mass spectrometer (CA-IRMS) at Cornell University Stable Isotope Laboratory (Ithaca, NY 14853 U.S.A.).

2.3. Water Adsorption−Desorption Measurements. Clay slurries were freeze-dried and pretreated at 105 °C for 24 h under vacuum (heating ramp rate of 1 °C per min to a final pressure of $\sim 10^{-4}$ Pa) to remove all water content. The exact mass was taken after the procedure for the calculation of water adsorption per mass of the dry clay sample. Helium gas was used to measure the dead volume of the system before a water vapor sorption isotherm was completed at 298 K. Water vapor within the sample was increased incrementally until maximum adsorption was reached and then lowered incrementally via vacuum until all water was desorbed. Water adsorption and desorption experiments were performed on a BELSORP-Max high precision gas/vapor adsorption apparatus from BEL Japan, Inc. (Toyonaka-city, Osaka, Japan). The system used two pressure sensors to ensure complete coverage of the pressure range along the isotherm. The system is purged with N_2 after each sample. Samples were analyzed using the BELMaster analysis program.

2.4. X-ray Diffraction Measurements and Modeling. The clay slurries following supernatant removal were pipetted onto a flat sample holder and equilibrated for at least 8 h at 95% RH before data collection. After recording the XRD profile at 95% RH, XRD profiles were recorded at decreasing moisture conditions (90, 80, 70, 60, 50, 40, 30, and 20% RH) by subjecting each sample to 1 h *in situ* equilibration at each RH value, while maintaining a constant temperature of 25 °C in the XRD sample chamber. The XRD profiles were recorded with a Bruker D8 Advance X-ray diffractometer operated at 40 kV and 40 mA. The diffractometer was equipped with a CHC+ humidity-controlled chamber (Anton Paar, Graz, Austria) coupled to an MHG humidity generator (ProUmid, Ulm, Germany). Scanning parameters were set at 0.02° 2θ step size with an 8 s counting time per step over a 1.5−8.5 2θ Cu Kα angular range (λ = 1.5418 Å).

The experimental patterns of MONT without and with glucose or cellobiose were modeled in the 3−11° 2θ Cu Kα range using the algorithms developed by Sakharov and coworkers[77] to determine the relative abundance layer types for 0W from 0.96 to 1.07 nm, 1W from 1.18 to 1.29 nm, 2W from 1.45 to 1.58 nm, and 3W from 1.8 to 1.95 nm.[39] Instead of designating the different interlayer nanopores as 0 to 3W the nanopore spacing is referred to by the nanometer width due to the uncertainty of the proportion of spacing attributed to the organic molecules versus that to the water population. Using Bragg's law, $n\lambda = 2d \sin\theta$, interlayer d-spacing can be related to the placement of the d_{001} peak along the 2θ axis.[38,39,61] The approach adopted to model the XRD nanopore abundance, which has been explained in detail elsewhere,[65] is described briefly here. One structure containing one or multiple different layer types was first used to reproduce the 001-reflection region as much as possible. When necessary, additional interstratified contributions containing 2W-layer or 3W-layer types were added to the structure model. In all samples, the quantification of nanopore abundance was determined from the consideration of three-layer types associated with different nanopore sizes. Only the change of proportion of these layers in the different samples was responsible of the good fit obtained for all patterns. For all patterns, structural parameters, such as the number of and relative abundance of the different interstratified structures (limited to four here), their composition (relative proportions of the different layer

DOI: 10.1021/acs.jpcc.9b09246
J. Phys. Chem. C 2019, 123, 28816−28827

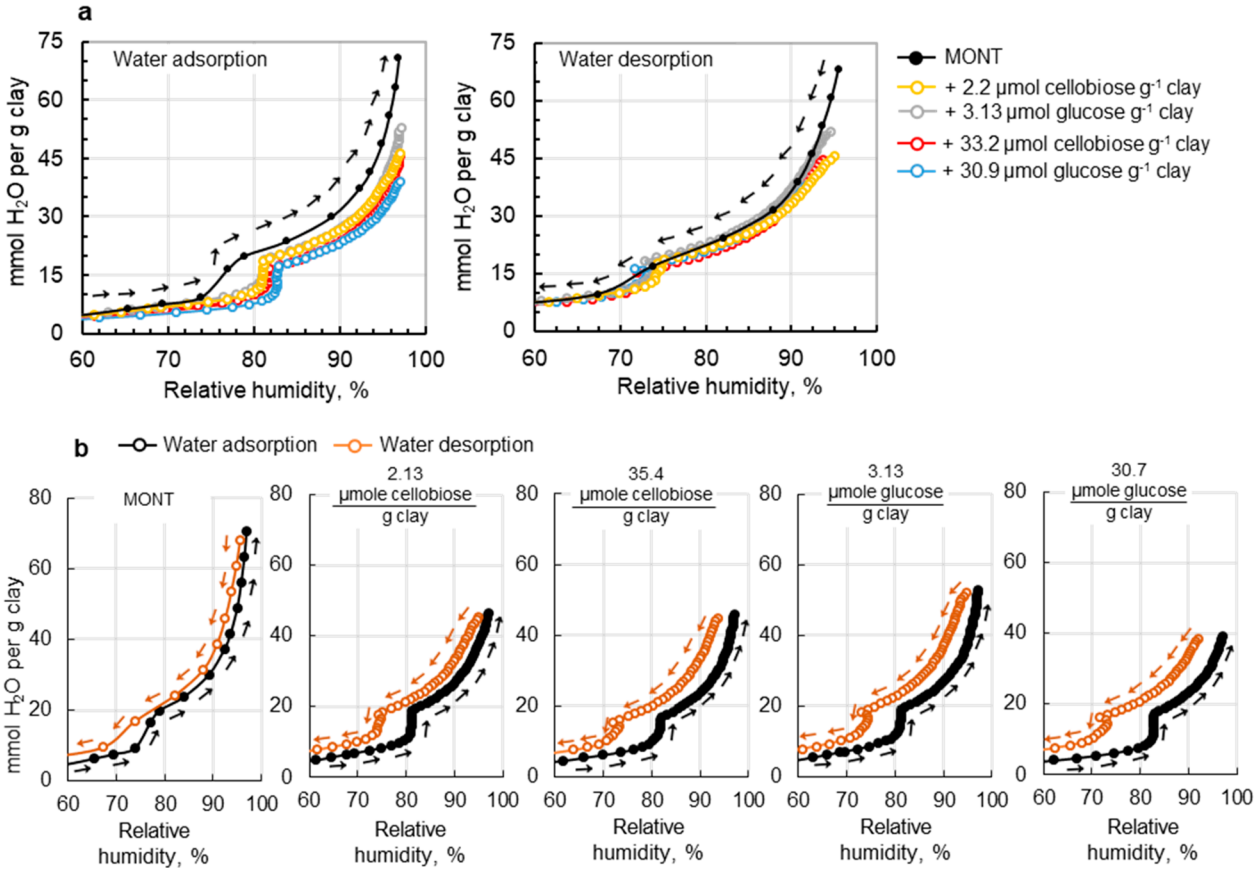

Figure 2. Carbohydrate-influenced water adsorption and desorption in montmorillonite (MONT). (a) Isotherms of water adsorption (left) and desorption (right) as a function of relative humidity obtained for montmorillonite alone or with different carbohydrate loadings with arrows showing direction of adsorption or desorption. (b) Comparison of water adsorption versus desorption profiles at each carbohydrate loading. All graphs are corrected for carbohydrate content (per gram dry clay with carbohydrate subtracted). Full profiles, including data at 20−60% relative humidity, are shown in Supporting Information, part B.

types), and the mean number of layers in the coherent scattering domain size along the *c**-axis, were adjusted to fit the experimental XRD pattern. The mean number of layers in the coherent scattering domain sizes was found to range between 12 and 7.5 layers for all patterns investigated and showed systematic increase with decreasing RH values, in agreement with previous studies on smectite structure evolution along water desorption isotherms.[38,65] Within the model, an "inert" phase was found at approximately 1.0 nm. This phase was present in all samples and did not change in intensity therefore was corrected for and considered to be an impurity.

2.5. FTIR Measurements. The samples were equilibrated for a minimum of 24 h at 11, 33, 53, 75, 95, or 99% RH using salt chambers with, respectively, LiCl, $MgCl_2$, $Mg(NO_3)_2$, NaCl, KNO_3, and K_2SO_4 as the salt used in a supersaturated mixture with DI water to maintain the RH condition in the chambers. Within the chambers, the RH was checked with a humidity probe. The RH-equilibrated samples were then transferred onto the ATR crystal followed by immediate data acquisition. In addition, with samples first equilibrated at 95% RH, we recorded kinetic ATR-FTIR data at 10 min intervals between scan acquisition for a duration of 100 min of air drying under ambient conditions. All FTIR measurements were recorded on a Thermo scientific Nicolet iS10 equipped with a smart iTR attachment and a diamond crystal. Spectra were collected from 3900 to 600 cm^{-1} with 32 coadded scans at 6 cm^{-1} resolution. OMNIC software (version 8.0) was used to record the spectra with automatic atmospheric CO_2 correction.

3. RESULTS AND DISCUSSION

3.1. Dynamics of Water Adsorption−Desorption in the Presence of Adsorbed Carbohydrates. In the absence of the carbohydrates, the water adsorption isotherm was in agreement with previously reported stepwise nonhomogeneous water adsorption on MONT.[63,64,69] For MONT alone, there was first a gradual increase in adsorbed water content from 20 to 74% RH, reaching 9.3 mmol of water g^{-1} of clay, followed by a steep increase in water content, jumping from 9.3 to 20.0 mmol of water g^{-1} of clay after only a 5% increase in RH from 74% RH to 79% RH (Figure 2a). A subsequent increase in RH led to a gradual increase in adsorbed water up to 41.5 mmol of water g^{-1} of clay at 93.6% RH (Figure 2a). At higher RH conditions, the water adsorption profile underwent a near-vertical increase, reflecting interparticle micropore water adsorption,[64,65] reaching an eventual maximum of 70.7 mmol of H_2O g^{-1} of clay at ~97% RH (Figure 2a). Notably, at 95% RH, we found that the adsorbed water amount of 48.79 mmol of water g^{-1} of clay for MONT alone was up to 3 times higher than previously reported values of 13.9−25 mmol of water g^{-1} of clay at 95% RH.[3,19,37,63,64,69] The use of a high-Na background electrolyte solution may account for this

DOI: 10.1021/acs.jpcc.9b09246
J. Phys. Chem. C 2019, 123, 28816−28827

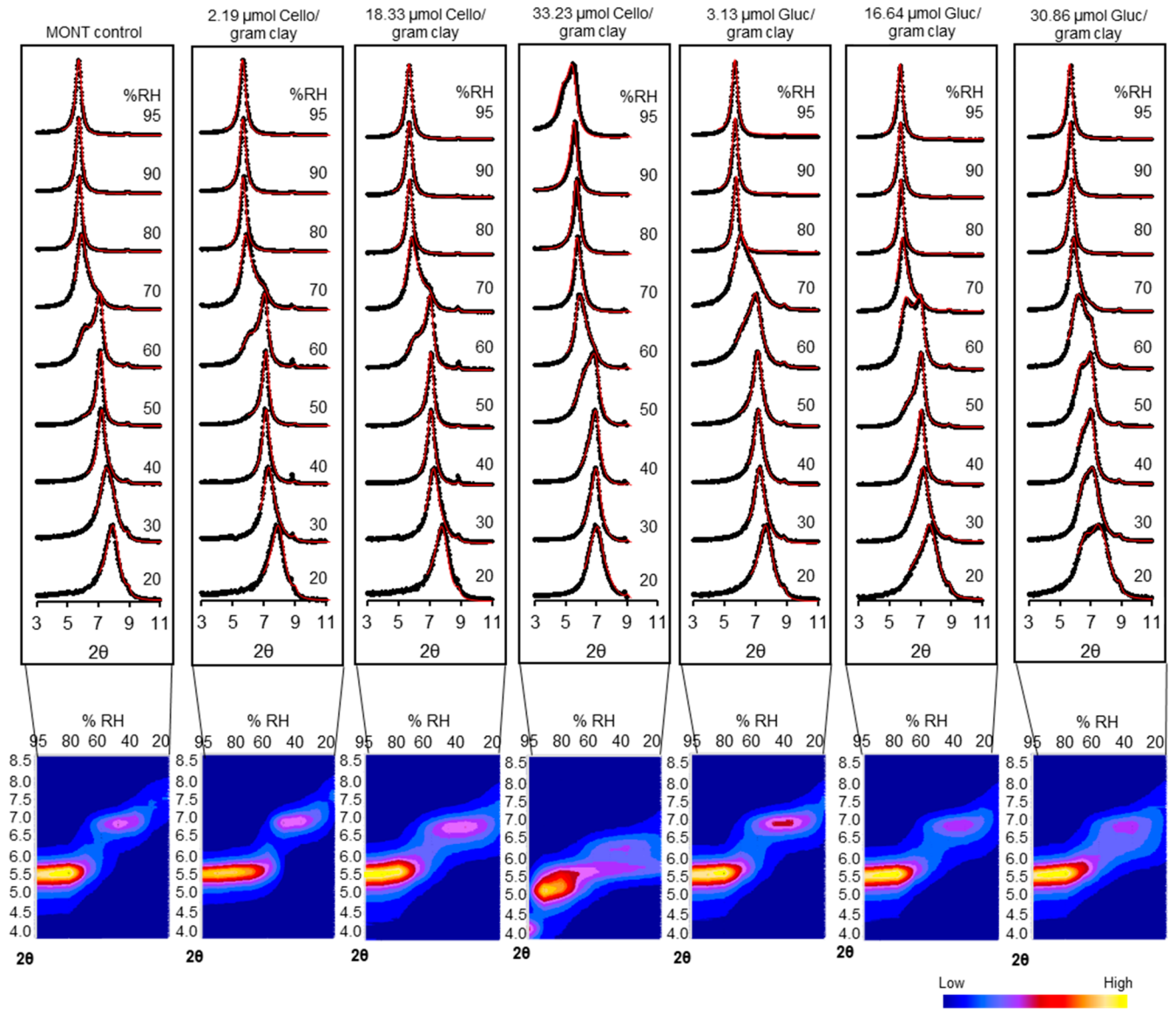

Figure 3. Moisture-dependent X-ray diffraction (XRD) profiles of nanopore width. The top panels show the XRD patterns (as black symbols) and associated model fits (red lines) of montmorillonite alone or loaded with cellobiose or glucose. The adsorbed amounts are shown in micromoles of carbohydrate per gram of dry clay). Samples were conditioned at different relative humidity (RH), from top to bottom: 95%, 90%, 80%, 70%, 60%, 50%, 40%, 30%, and 20%. The bottom panels show the three-dimensional surface maps of the X-ray diffraction patterns; the color gradient presents the intensity of the XRD data. The full set of collected XRD patterns is provided in the Supporting Information, part C.

discrepancy because increasing Na concentration was previously reported[37] to promote water adsorption on MONT.

In the presence of the adsorbed carbohydrates, two major differences were notable in the water adsorption profiles. First, there was a decrease in the near-vertical portion of the profile (above 90% RH), indicating both a decrease in micropore interparticle water and confinement of water adsorption mostly within nanopore regions in the carbohydrate−MONT aggregates. As a result, relative to MONT alone, the maximum adsorbed water content in carbohydrate-containing samples was lower by 23−35 mmol of H_2O g^{-1} of clay with adsorbed glucose or cellobiose (Figure 2b). Second, higher RH conditions were needed with the carbohydrate-containing samples to achieve the same amount of adsorbed water obtained with MONT alone, indicating that higher water activity was required to hydrate the carbohydrates−MONT aggregates than to hydrate the Na-saturated MONT. (Figure 2b). However, evidence of hysteresis, which is characterized by higher water content in the desorption profile than in the adsorption profile at the same equilibrated RH condition, was found to be more pronounced in the presence of adsorbed carbohydrates (Figure 2b). Due to this difference in the extent of hysteresis, the net water loss on the desorption curve was greater for MONT alone than for the MONT−carbohydrate samples (Figure 2b). To probe further the distribution dynamics of both hydrated nanopores and water populations within the carbohydrate−MONT aggregates, we obtained XRD data and vibrational spectroscopic data, respectively.

3.2. Moisture-Dependent Interstratification Patterns and Nanopore Size Distribution. To investigate nanopore size dynamics at the different moisture conditions, we obtained XRD patterns under RH-controlled conditions (Figure 3 and Tables 1 and 2). The patterns for MONT alone matched previous reports of the stepwise decrease of the d_{001} peak

DOI: 10.1021/acs.jpcc.9b09246
J. Phys. Chem. C 2019, 123, 28816−28827

Table 1. Results from Adsorption Experiments and Experimental X-ray Diffraction Patterns of Montmorillonite Reacted with Cellobiose[a,b]

	amount adsorbed											
	0 μmol g^{-1} of clay			2.19 μmol g^{-1} of clay			18.3 μmol g^{-1} of clay			33.2 μmol g^{-1} of clay		
% RH	d_{001}	Δd	fwhm	d_{001}	Δd	fwhm	d_{001}	Δd	fwhm	d_{001}	Δd	fwhm
95	1.55		0.39	1.55		0.45	1.55		0.43	1.59		0.92
90	1.55	0.007	0.39	1.55	0.003	0.44	1.54	0.009	0.44	1.57	0.022	0.39
80	1.54	0.015	0.39	1.54	0.012	0.44	1.52	0.025	0.47	1.52	0.065	0.39
70	1.50	0.057	0.71	1.49	0.064	0.89	1.49	0.055	0.79	1.52	0.071	0.39
60	1.26	0.296	0.77	1.26	0.293	0.77	1.29	0.258	1.3	1.49	0.096	0.71
50	1.25	0.302	0.43	1.26	0.297	0.46	1.27	0.281	0.66	1.28	0.304	0.77
40	1.24	0.315	0.59	1.25	0.308	0.53	1.27	0.283	0.61	1.27	0.315	0.62
30	1.17	0.382	0.92	1.22	0.332	0.81	1.26	0.291	0.79	1.27	0.321	0.79
20	1.12	0.429	0.79	1.14	0.419	0.99	1.21	0.339	1.4	1.25	0.338	1.4

[a]RH, relative humidity (RH) for *in situ* moisture-dependent X-ray diffraction measurements; fwhm, full width at half-maximum; d_{001}, the basal spacing of the clay layers shown in nm; Δd, difference in interlayer spacing relative to the highly hydrated sample (at 95% RH). [b]Full data sets are shown in Supporting Information, part A.

Table 2. Results from Adsorption Experiments and Experimental X-ray Diffraction Patterns of Montmorillonite reacted With Glucose[a,b]

	amount adsorbed											
	0 μmol g^{-1} of clay			3.13 μmol g^{-1} of clay			16.6 μmol g^{-1} of clay			30.9 μmol g^{-1} of clay		
% RH	d_{001}	Δd	fwhm	d_{001}	Δd	fwhm	d_{001}	Δd	fwhm	d_{001}	Δd	fwhm
95	1.55		0.39	1.56		0.41	1.55		0.41	1.55		0.41
90	1.55	0.007	0.39	1.55	0.013	0.40	1.54	0.003	0.41	1.54	0.005	0.40
80	1.54	0.015	0.39	1.53	0.030	0.40	1.53	0.017	0.39	1.54	0.009	0.41
70	1.50	0.057	0.71	1.45	0.115	1.2	1.49	0.057	0.64	1.49	0.054	0.63
60	1.26	0.296	0.77	1.26	0.296	1.0	1.26	0.287	1.5	1.41	0.138	1.4
50	1.25	0.302	0.43	1.25	0.315	0.58	1.26	0.291	0.62	1.28	0.264	1.2
40	1.24	0.315	0.59	1.24	0.324	0.61	1.25	0.302	0.57	1.27	0.278	1.0
30	1.17	0.382	0.92	1.22	0.341	0.71	1.23	0.318	0.85	1.27	0.281	1.3
20	1.12	0.429	0.79	1.15	0.410	0.88	1.16	0.391	1.2	1.19	0.360	1.8

[a]RH, relative humidity (RH) for *in situ* moisture-dependent X-ray diffraction measurements; fwhm, full width at half-maximum; d_{001}, the basal spacing of the clay layers shown in nm; Δd, difference in interlayer spacing relative to the highly hydrated sample (at 95% RH). [b]Full data set are shown in Supporting Information, part A.

position along the 2θ axis as a function of increased dehydration.[24,39,62] This stepwise decrease was accompanied by an oscillating evolution of the fwhm in MONT alone, which was at minimum for the d_{001} values corresponding to most homogeneous hydration states such as between 95% and 80% RH and increased in the transition zones due to the presence of interstratified interlayers (Figure 3 and Tables 1 and 2). The d_{001} position of MONT decreased from 1.55 nm at 95% RH to 1.12 nm at 20% RH (Figure 3). There was minimal change in both the d_{001} and fwhm values from 95% RH to 80% RH, after which the peak broadened from 0.39 to 0.71° 2θ (45% increase in fwhm) at 70% RH for MONT alone (Figure 3 and Tables 1 and 2). There was a decrease of 0.24 nm (a 16% drop) in d_{001} between 70% and 60% RH (Figure 3 and Tables 1 and 2). The peak was subsequently symmetrical at RH lower than 60% (Figure 3). At the low carbohydrate contents (3.13 μmol of glucose per g of clay and 2.19 μmol of cellobiose per g of clay) and midrange carbohydrate content (16.64 μmol of glucose per g of clay and 18.33 μmol of cellobiose per g of clay), the evolution of XRD patterns was in close agreement with that of MONT alone (Figure 3). At about 8−9 times higher glucose content (30.86 μmol of glucose/g of clay), there was both a broadening of the d_{001} peak from 50% to 20% RH (fwhm increased from 1.2 to 1.8° 2θ) and an appreciable expansion (about 7%) of the interlayer size (from 1.28 to 1.19 nm); there were no major differences in the d_{001} peak at the high RH levels (95%, 90%, and 80% RH) (Figure 3 and Table 2). With 12−15 times higher cellobiose content (33.23 μmol g^{-1} of clay), the pattern was similar to the high glucose content sample (Figure 3 and Table 1). High glucose and high cellobiose content samples both revealed an expanded layer-to-layer distance at 20% RH (1.25 and 1.19 nm in cellobiose and glucose, respectively) compared to 1.12 nm in MONT alone (Figure 3). Moreover, at 20% RH, the high carbohydrate content samples showed more broad peaks (fwhm of 1.4 and 1.8° 2θ) compared to MONT alone (0.79° 2θ) (Figure 3 and Tables 1 and 2). Our results of an increase in interlayer nanopore with increasing adsorbed carbohydrate were in agreement with published results with MONT populated with lactose, a disaccharide composed of glucose and galactose.[78]

Three-dimensional illustrations of the XRD patterns highlighted the influence of carbohydrate adsorption on the MONT interlayer dynamics (Figure 3). The intensity profiles of the low cellobiose (2.19 μmol g^{-1} of clay) and low glucose (3.13 μmol g^{-1} of clay) samples were similar to the intensity distribution of MONT alone (Figure 3). The area where the peak intensity was highest was between 95 and 80% RH (Figure 3). This region between 95 and 80% RH also showed

DOI: 10.1021/acs.jpcc.9b09246
J. Phys. Chem. C 2019, 123, 28816−28827

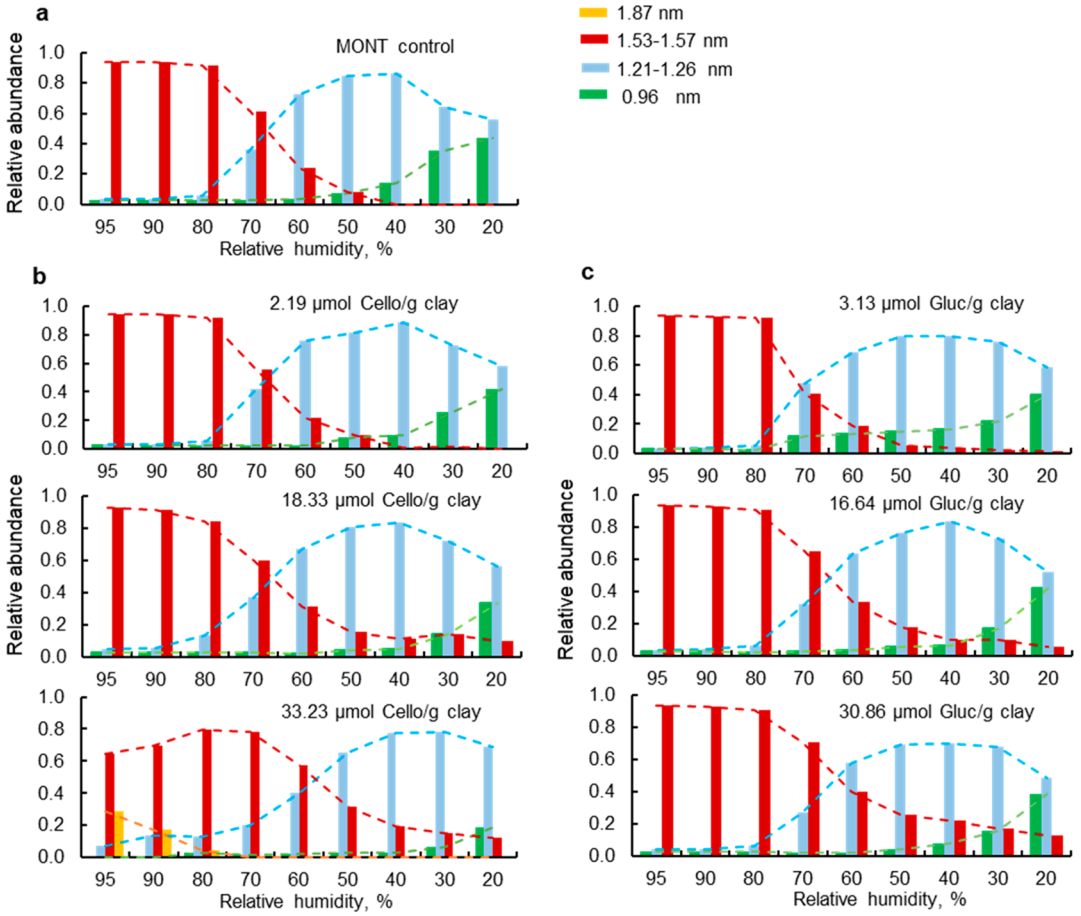

Figure 4. Modeling moisture-dependent X-ray diffraction profile of nanopore distribution. Relative nanopore abundance of (a) montmorillonite alone or loaded with (b) cellobiose or (c) glucose. In parts b and c, loadings are shown in micromoles of carbohydrate per gram of dry clay. The different interlayer sizes used in the modeling are represented by green bars (0.96 nm), light blue bars (1.21−1.26 nm), dark red bars (1.53−1.57 nm), and yellow bars (1.87 nm). Additional modeling results are shown in Supporting Information, part D.

the least fluctuation in d_{001} and fwhm values (Figure 3 and Table 1). At ∼70% RH, a low-intensity transition occurred followed by a second high-intensity area from 60 to 20% RH (Figure 3). Samples with high carbohydrate content (33.23 μmol of cellobiose/g clay and 30.86 μmol of glucose) had less of a transition between the two high-intensity areas (Figure 3). The sample with the highest cellobiose content (33.23 μmol g^{-1} of clay) exhibited a third area of intensity at 95% RH, which corresponded to interlayer expansion and peak broadening recorded by the XRD patterns at 95% RH (Figure 3 and Table 1).

3.3. Quantitative Profiling of Interlayer Nanopore Expansion. Under the different conditions, we employed XRD modeling to quantify the relative abundance of the different nanopore sizes (Figure 4): 0.96 nm (small-sized), 1.21−1.26 nm (medium-sized), 1.53−1.57 (large-sized), and 1.87 nm (largest-sized). Similar to prior XRD profile modeling of cation-saturated MONT samples as a function of decreasing RH,[38,62] we found an increased abundance of the small-sized nanopore at the expense of the collapse of the medium-sized and large-sized nanopores both in the presence and absence of adsorbed glucose or cellobiose (Figure 4b,c). However, the relative abundance of the specific nanopore sizes was depended on whether or not the carbohydrates were present (Figure 4).

For MONT alone, we obtained a homogeneous distribution of the large-sized nanopores from 95% RH to 80% RH (Figure 4a). The medium-sized nanopores became more prevalent from 70% to 40% RH but, from 40% to 20% RH, further nanopore collapse was highlighted by the increase in the abundance of the small-sized nanopores, from 14% to 44% (Figure 4a). At 50% RH, only 8% of the clay interlayers were dehydrated (small-sized nanopore) (Figure 4a).

At relatively lower RH conditions, particularly below 40% RH, samples showed heterogeneous distributions of the different nanopore sizes and the specific distribution of the nanopore sizes was dependent on carbohydrate content (Figure 4). At 20% RH, in MONT alone or at low carbohydrate contents (3.13 μmol of glucose per g of clay and 2.19 μmol of cellobiose per g of clay), approximately 60% of the nanopores were medium-sized and 40% were small-sized (Figure 4). We note that, consistent with a high heterogeneity of nanopore size distribution at low RH determined from the XRD modeling, much larger fwhm values were determined from the experimental XRD patterns of MONT with high carbohydrate content (Table 1 and Figure 4). With relatively higher carbohydrate content samples (33.23 μmol of cellobiose per g of clay and 30.86 μmol of glucose per g of clay) at 20% RH, there was up to 13% abundance of the large-sized nanopores, with an accompanying decrease in small- and medium-sized nanopores (Figure 4b,c). By contrast, at high RH (95% to 80%), the modeling determined a homogeneous distribution of the large-sized nanopore in both the absence

DOI: 10.1021/acs.jpcc.9b09246
J. Phys. Chem. C 2019, 123, 28816−28827

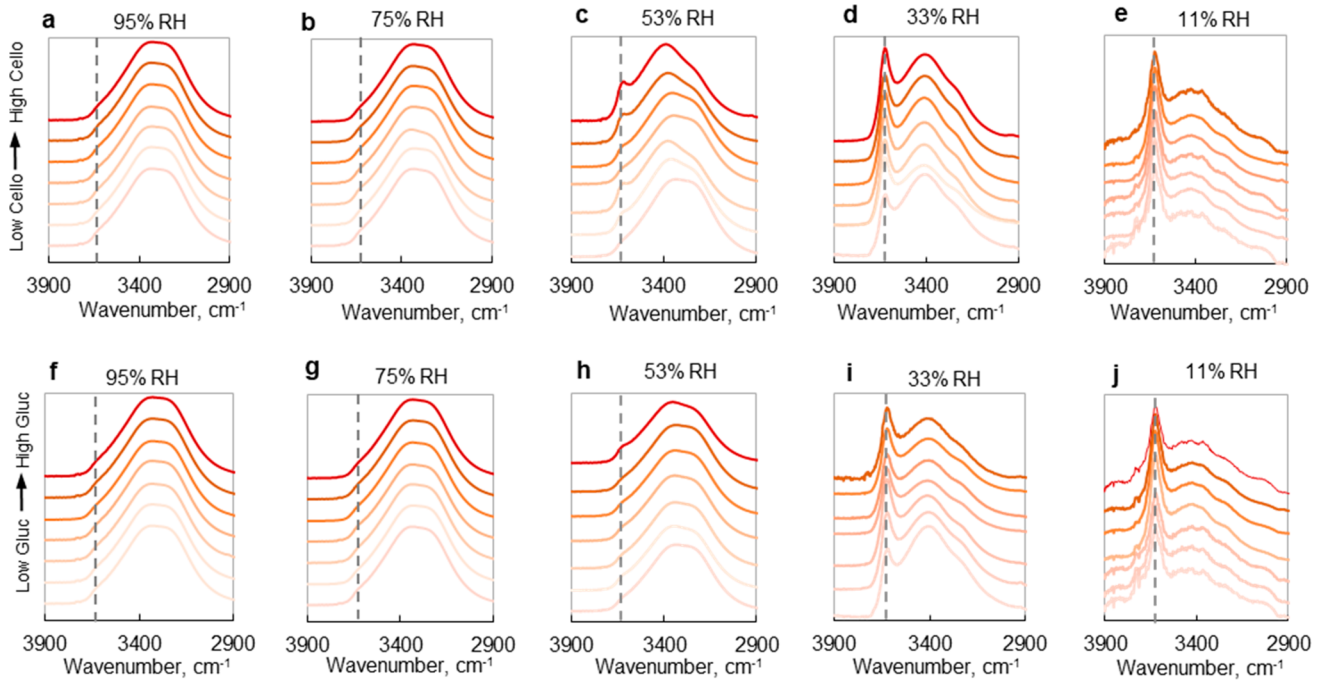

Figure 5. Loss of exchangeable water during dehydration in carbohydrate-smectite nanoaggregates. ATR-FTIR spectra of MONT in the presence of increasing carbohydrate concentrations of cellobiose (a)−(e) or glucose (f)−(j) equilibrated at different RHs (from left to right: 95% RH, 75% RH, 53% RH, 33% RH, 11% RH). From the bottom to the top of of parts a−e are the spectra of MONT loaded with cellobiose (μmol of cellobiose/g of dry clay) 0, 2.19, 2.64, 4.14, 18.33, and 33.23 μmol/g; from the bottom to the top of of parts f−j are the spectra of MONT loaded with glucose (μmol of glucose/g of dry clay) 0, 3.13, 3.42, 3.47, 16.64, and 30.86 μmol/g. The spectra are showing the νOH stretching region of the water bands: mineral −OH is represented by the sharp peak at ~3615 cm^{-1}; the exchangeable water population is represented by the broad peak at 3530−3050 cm^{-1}. All spectra were normalized to the maximum reflectance. The full recorded spectra (4000−600 cm^{-1}) for cellobiose−MONT and glucose−MONT samples are provided in Supporting Information, part E and part F, respectively.

and presence of carbohydrates (Figure 4). The only exception to this homogeneity is the additional presence of the largest-size nanopore (1.87 nm) at the highest cellobiose content of 33.23 μmol of cellobiose per g of clay; this nanopore size was not present at similar glucose content (Figure 4b). This finding implied that the structure of the carbohydrate may influence the nanopore restructuring. To gain more insight on this phenomenon, further investigation is needed with a greater variety of carbohydrate structures. In sum, our XRD profiling as a function of dehydration revealed that greater nanopore sizes were maintained when carbohydrate content was high, despite a near-similar water content at all investigated conditions based on our water desorption profiles (Figure 2 and Figure 4).

3.4. Exchangeable Water Population in the Absence and Presence of Adsorbed Carbohydrates. To investigate further the influence of the adsorbed carbohydrates on the MONT water dynamics, we performed FTIR analysis (3900−2900 cm^{-1}) on samples equilibrated at five RH conditions: 95%, 75%, 53%, 33%, and 11% RH (Figure 5). In agreement with previous studies,[3,63,68,70−72] we found a decrease in the exchangeable water band relative to the mineral OH band as a function of increasing dehydration (Figure 5). The mineral νOH band was not visible at both 95% and 75% RH in the presence and absence of carbohydrates because the FTIR signature of the exchangeable water νOH band overwhelmed the νOH of the mineral structure (Figure 5a,b,f,g). However, previous studies[3,63,68] found the structural νOH band was still visible alongside the exchangeable OH band at 90%−94% RH (Figure 5a,f). At 53% RH, the mineral νOH band was noticeable in all the cellobiose-containing samples but only visible at the highest glucose concentration (30.86 μmol glucose/g dry clay) (Figures 5d−j). At 33% RH, the samples with the highest carbohydrate loadings were also found to exhibit the most depletion in the relative intensity of the exchangeable water νOH band (Figure 5d,i). With samples equilibrated at 11% RH, the exchangeable water νOH band was significantly depleted, leading to the prominence of the mineral νOH band (Figure 5e,f). At this dry condition, however, the influence of the adsorbed carbohydrate on the relative abundance of the two νOH bands were not as noticeable as in the higher RH condition (Figure 5e,j). In sum, these data indicated that, at the same RH condition (53% or less), the presence of glucose and cellobiose led to a decrease in the relative abundance of exchangeable waters within the MONT aggregate (Figure 5).

In addition to the aforementioned FTIR measurements on RH-controlled samples, we monitored the kinetics of FTIR-determined water populations during the drying of highly hydrated samples, initially equilibrated at 95% RH (Figure 6). We monitored the intensity of the exchangeable water νOH peak relative to the νOH peak of the mineral structure (Figure 6). This ratio was set to zero when the FTIR signature of the exchangeable water νOH band overwhelmed the νOH band of the mineral structure (i.e., at very high moisture content). In MONT alone, the mineral νOH was only quantifiable after 60 min of drying because exchangeable water saturated the mineral surface prior to 60 min; at 60 min, the initial ratio of mineral to exchangeable water OH intensities was 0.33 (Figure 6b−d). Due to the increasing depletion of the exchangeable waters within MONT alone, the ratio increased to 1.8 by the end of recorded drying time, 100 min (Figure 6b−d).

DOI: 10.1021/acs.jpcc.9b09246
J. Phys. Chem. C 2019, 123, 28816−28827

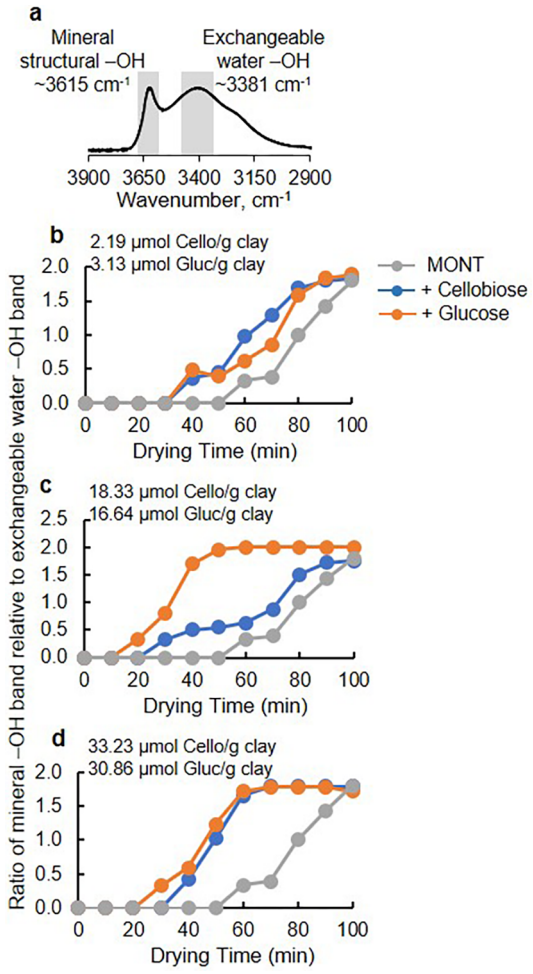

Figure 6. Drying time-dependent water populations determined by Fourier-transform infrared spectroscopy. (a) Representative FTIR spectrum illustrating the two −OH vibrational bands of interest. (b)−(d) The ratio of mineral −OH vibrational band at ∼3615 cm^{-1} to the exchangeable water −OH vibrational band at ∼3530−3050 cm^{-1} for MONT alone and loaded (μmol of compound/weight of dry clay) with (b) 2.19 μmol of cellobiose, 3.13 μmol of glucose; (c) 18.33 μmol of cellobiose, 16.64 μmol of glucose; and (d) 33.23 μmol of cellobiose, 30.86 μmol of glucose. All samples were equilibrated at 95% RH prior to drying and time points were taken at 10 min intervals. The FTIR spectra and the determined peak intensities are Supporting Information, part G.

Compared to MONT alone, the data obtained with MONT populated with either carbohydrate compound indicated a faster depletion in the relative abundance of exchangeable waters (Figure 6b−d). Specifically, the ratio of the mineral νOH band to exchangeable water νOH band in the presence of adsorbed glucose or cellobiose was quantifiable after only 10−30 min of drying time, i.e., 20−40 min earlier than the corresponding time of MONT alone (Figure 6b−d). The faster kinetics of exchangeable water loss may be due to possible lower hydration energy for carbohydrates in the MONT−carbohydrate samples than for Na in the MONT alone attributed, respectively, to dipole−dipole interactions versus ion−dipole interactions. In accordance with this proposal, our water adsorption profile showed that higher RH (i.e., higher water activity) was required to obtain similar amounts of water content within the MONT sample containing adsorbed carbohydrates on (Figure 2). Interestingly, the final ratio value at 100 min drying time was very similar in both the absence and presence of carbohydrates, about 1.8−2.0, which agreed with the similar water content obtained with the desorption profiles at low RH (Figure 2; Figure 6b,d).

4. CONCLUSION

In this study we sought to evaluate two hypotheses: (1) expanded nanopore size of MONT−carbohydrate aggregate due to water trapping and (2) enhanced water trapping within MONT−carbohydrate aggregates due to increased interactions with water molecules. Analysis of moisture-dependent XRD patterns provided quantitative evidence in support of an expanded mineral nanopore size in MONT enriched with adsorbed carbohydrates. We propose that carbohydrates prevented collapse of the mineral interlayer by acting as pillars within the interlayer nanopores. In accordance with this proposal, a recent molecular dynamics study has illustrated hydrogen-bonded aggregation of carbohydrates within MONT interlayers.[67] Our XRD data could not resolve the role or lack thereof of water molecules associated with the carbohydrates in contributing to the nanopore expansion. However, water adsorption data revealed that higher water activity was needed to obtain the same amount of adsorbed water in carbohydrate-containing samples compared to MONT alone, implying lower hydration energy for carbohydrates in the MONT−carbohydrate composites than for Na in the MONT alone. It was reported previously[79,80] that waters associated with disaccharides and polysaccharides had slower kinetic motion than waters associated with glucose. Here, in highly hydrated samples (i.e., at RH > 80%), we found the nanopore sizes of MONT populated with the cellobiose (a disaccharide) were larger than MONT populated with glucose (a monosaccharide), which may be due to enhanced water trapping by cellobiose relative to glucose. Carminati et al.[60] have proposed that secretion of organic compounds by plant roots may be responsible for enhanced retention of soil moisture in the vicinity of the rhizosphere. Interestingly, we found that the trend in the water holding capacity of the carbohydrate-populated clays as a function of dehydration depended on the dehydration procedure. On one hand, during gradual stepwise dehydration, the water loss at each subsequent equilibrated moisture condition was greater for MONT alone than for carbohydrate−MONT samples. On the other hand, time-resolved infrared analysis determined faster loss of exchangeable water during rapid dehydration (i.e., air drying) in the presence of carbohydrates. Further investigation is needed to understand the influence of carbohydrate hydration dynamics on water trapping dynamics during gradual versus rapid dehydration of smectite interlayer nanopores. Here our data demonstrate that smectite-type clays enriched in adsorbed carbohydrates can induce restructuring and expansion of the mineral nanopores as well as dynamic changes in water content and water trapping. Important next steps to build on the findings in the present study are spectroscopic investigations of carbohydrate−clay interactions and follow-up studies of hydration dynamics with different carbohydrate structures and cations populating the smectite-interlayer nanopores.

■ ASSOCIATED CONTENT

Supporting Information

The Supporting Information is available free of charge on the ACS Publications website at DOI: 10.1021/acs.jpcc.9b09246.

DOI: 10.1021/acs.jpcc.9b09246
J. Phys. Chem. C 2019, 123, 28816−28827

Extended table listing d_{001} and fwhm values for XRD profiles of all glucose and cellobiose concentrations including those shown in Table 1 (part A), extended graphs of water adsorption−desorption profiles which show 20% RH-100% RH, instead of 60−100% as shown in Figure 2 (part B), unprocessed XRD profiles of all concentrations of glucose and cellobiose a selection of which is shown in Figure 3 (part C), XRD profile modeling of remaining concentrations of glucose and cellobiose not shown in Figure 4 (part D), full FTIR spectra (4000−600 cm^{-1}) of RH equilibrated MONT−cellobiose samples shown in Figure 5 (part E), full FTIR spectra (4000−600 cm^{-1}) of RH equilibrated MONT−glucose samples shown in Figure 5 (part F), table of values ratios where determined from (intensity of mineral and exchangeable water populations) in Figure 6 as well as FTIR spectra for each kinetic time point from 0 to 100 min for all glucose and cellobiose concentrations, not only those shown in Figure 6 (part G), ATR-FTIR spectra (PDF)

AUTHOR INFORMATION

Corresponding Author

*Email: ludmilla.aristilde@northwestern.edu. Phone: 847-491-2999.

ORCID

Bruno Lanson: 0000-0003-1187-3221

Ludmilla Aristilde: 0000-0002-8566-1486

Notes

The authors declare no competing financial interest.

ACKNOWLEDGMENTS

Graduate support for S.E.K. at Cornell University was provided by the NSF Graduate Research and Training (IGERT) program in Cross-Scale Biogeochemistry and Climate and a NSF grant awarded to L.A. (CHE #1646815). Travel support for S.E.K. to work at the Université Grenoble Alpes was provided by the Chateaubriand Fellowship from the Embassy of France in the United States, the Cornell Graduate School Research Travel Grant, and the Einaudi Center International Research Travel Award from the Mario Einaudi Center for International Studies at Cornell University. We are grateful to Dr. Alex Fernandez-Martinez and Valérie Magnin at the Institut des Sciences de la Terre (ISTerre) at the Université Grenoble Alpes for, respectively, assistance with the FTIR measurements and conducting the water adsorption isotherms. We thank Kim Sparks of the Cornell University Stable Isotope Laboratory and Tatyana Dokuchayeva at the Cornell Nutrient Analysis Laboratory and Dr. Eleanor Bakker for providing the molecular dynamics snapshot of MONT−glucose system used as the graphical abstract. S.E.K. acknowledges helpful discussions with members of her doctoral thesis committee, Dr. Murray McBride (Cornell University) and Dr. Taryn Bauerle (Cornell University).

REFERENCES

(1) Jackson, M. L. Frequency Distribution of Clay Minerals in Major Great Soil Groups as Related to the Factors of Soil Formation. *Clays Clay Miner.* **1957**, *6* (1), 133−143.

(2) Ross, C. S.; Hendricks, S. B. *Minerals of the Montmorillonite Group; Their Origin and Relation to Soils and Clays*; USGS, 1945; DOI DOI: 10.3133/pp205B.

(3) Schuttlefield, J. D.; Cox, D.; Grassian, V. H. An Investigation of Water Uptake on Clays Minerals Using ATR-FTIR Spectroscopy Coupled with Quartz Crystal Microbalance Measurements. *J. Geophys. Res.* **2007**, *112* (21), 1−14.

(4) Claquin, T.; Schulz, M.; Balkanski, Y. J. Modeling the Mineralogy of Atmospheric Dust Sources. *J. Geophys. Res. Atmos.* **1999**, *104* (D18), 22243−22256.

(5) Sokolik, I. N.; Toon, O. B. Incorporation of Mineralogical Composition into Models of the Radiative Properties of Mineral Aerosol from UV to IR Wavelengths. *J. Geophys. Res. Atmos.* **1999**, *104* (D8), 9423−9444.

(6) Kalderon-Asael, B.; Erel, Y.; Sandler, A.; Dayan, U. Mineralogical and Chemical Characterization of Suspended Atmospheric Particles over the East Mediterranean Based on Synoptic-Scale Circulation Patterns. *Atmos. Environ.* **2009**, *43* (25), 3963−3970.

(7) Moreno, T.; Querol, X.; Castillo, S.; Alastuey, A.; Cuevas, E.; Herrmann, L.; Mounkaila, M.; Elvira, J.; Gibbons, W. Geochemical Variations in Aeolian Mineral Particles from the Sahara-Sahel Dust Corridor. *Chemosphere* **2006**, *65* (2), 261−270.

(8) Odom, I. Smectite Clay-Minerals Properties and Uses. *Philos. Trans. R. Soc., A* **1984**, *311* (1517), 391.

(9) del Hoyo, C.; Rive, V.; Vincente, M. A. Adsorption of Melted Drugs onto Smectite. *Clays Clay Miner.* **1996**, *44* (3), 424−428.

(10) Thiebault, T.; Guégan, R.; Boussafir, M. Adsorption Mechanisms of Emerging Micro-Pollutants with a Clay Mineral: Case of Tramadol and Doxepine Pharmaceutical Products. *J. Colloid Interface Sci.* **2015**, *453*, 1−8.

(11) Tian, S.; Jiang, P.; Ning, P.; Su, Y. Enhanced Adsorption Removal of Phosphate from Water by Mixed Lanthanum/Aluminum Pillared Montmorillonite. *Chem. Eng. J.* **2009**, *151* (1−3), 141−148.

(12) Hamza, W.; Dammak, N.; Hadjltaief, H. B.; Eloussaief, M.; Benzina, M. Sono-Assisted Adsorption of Cristal Violet Dye onto Tunisian Smectite Clay: Characterization, Kinetics and Adsorption Isotherms. *Ecotoxicol. Environ. Saf.* **2018**, *163* (June), 365−371.

(13) Kausar, A.; Iqbal, M.; Javed, A.; Aftab, K.; Nazli, Z. i. H.; Bhatti, H. N.; Nouren, S. Dyes Adsorption Using Clay and Modified Clay: A Review. *J. Mol. Liq.* **2018**, *256* (March), 395−407.

(14) Nazir, M. S.; Haa, M.; Kassim, M.*Nanoclay Reinforced Polymer Composites*; Springer, 2016; pp 35−56.

(15) de Paiva, L. B.; Morales, A. R.; Valenzuela Díaz, F. R. Organoclays: Properties, Preparation and Applications. *Appl. Clay Sci.* **2008**, *42* (1−2), 8−24.

(16) Peretyazhko, T. S.; Sutter, B.; Morris, R. V.; Agresti, D. G.; Le, L.; Ming, D. W. Fe/Mg Smectite Formation under Acidic Conditions on Early Mars. *Geochim. Cosmochim. Acta* **2016**, *173*, 37−49.

(17) Michalski, J. R.; Cuadros, J.; Bishop, J. L.; Darby Dyar, M.; Dekov, V.; Fiore, S. Constraints on the Crystal-Chemistry of Fe/Mg-Rich Smectitic Clays on Mars and Links to Global Alteration Trends. *Earth Planet. Sci. Lett.* **2015**, *427*, 215−225.

(18) Che, C.; Glotch, T. D.; Bish, D. L.; Michalski, J. R.; Xu, W. Spectroscopic Study of the Dehydration and/or Dehydroxylation of Phyllosilicate and Zeolite Minerals. *J. Geophys. Res.* **2011**, *116* (5), 1−23.

(19) Frinak, E. K.; Mashburn, C. D.; Tolbert, M. A.; Toon, O. B. Infrared Characterization of Water Uptake by Low-Temperature Na-Montmorillonite: Implications for Earth and Mars. *J. Geophys. Res.* **2005**, *110* (D9), 7.

(20) Sposito, G. *The Chemistry of Soils*, second; Oxford University Press, 2008; DOI DOI: 10.1017/CBO9781107415324.004.

(21) Bourg, Ian C.; Sposito, Garrison; Bourg, A. C. M. Modeling Cation Diffusion in Compacted Water- Saturated Sodium Bentonite at Low Ionic Strength. *Environ. Sci. Technol.* **2007**, *41*, 8118−8122.

(22) Dazas, B.; Lanson, B.; Delville, A.; Robert, J. L.; Komarneni, S.; Michot, L. J.; Ferrage, E. Influence of Tetrahedral Layer Charge on the Organization of Interlayer Water and Ions in Synthetic Na-Saturated Smectites. *J. Phys. Chem. C* **2015**, *119* (8), 4158−4172.

(23) Ferrage, E.; Tournassat, C.; Rinnert, E.; Lanson, B. Influence of PH on the Interlayer Cationic Composition and Hydration State of Ca-Montmorillonite: Analytical Chemistry, Chemical Modelling and

XRD Profile Modelling Study. *Geochim. Cosmochim. Acta* **2005**, *69* (11), 2797−2812.
(24) Ferrage, E.; Lanson, B.; Sakharov, B. A.; Geoffroy, N.; Jacquot, E.; Drits, V. A. Investigation of Dioctahedral Smectite Hydration Properties by Modeling of X-Ray Diffraction Profiles: Influence of Layer Charge and Charge Location. *Am. Mineral.* **2007**, *92* (10), 1731−1743.
(25) Tertre, E.; Ferrage, E.; Bihannic, I.; Michot, L. J.; Prêt, D. Influence of the Ionic Strength and Solid/Solution Ratio on Ca(II)-for-Na+ Exchange on Montmorillonite. Part 2: Understanding the Effect of the m/V Ratio. Implications for Pore Water Composition and Element Transport in Natural Media. *J. Colloid Interface Sci.* **2011**, *363* (1), 334−347.
(26) Holmboe, M.; Bourg, I. C. Molecular Dynamics Simulations of Water and Sodium Di Ff Usion in Smectite Interlayer Nanopores as a Function of Pore Size and Temperature. *J. Phys. Chem. C* **2014**, *118*, 1001−1013.
(27) Ahmed, M. A.; Kroener, E.; Benard, P.; Zarebanadkouki, M.; Kaestner, A.; Carminati, A. Drying of Mucilage Causes Water Repellency in the Rhizosphere of Maize: Measurements and Modelling. *Plant Soil* **2016**, *407* (1−2), 161−171.
(28) Greenland, D. The Adsorption of Sugars by Montmorillonite II. *J. Soil Sci.* **1956**, *7* (2), 329−334.
(29) Greenland, D. J. Interaction between Clays and Organic Compounds in Soils Part II. Adsorption of Soil Organic Compounds and Its Effect on Soil Properties. *Soil Fertil.* **1965**, No. 2228, 521−532.
(30) Greenland, D. J.; Lindstrom, G. R.; Quirk, J. P. Organic Materials Which Stabilize Natural Soil Aggregates. *Soil Sci. Soc. Proc.* **1962**, *26*, 366−370.
(31) Olness, A.; Clapp, C. E. Influence of Polysaccharide Structure on Dextran Adsorption by Montmorillonite. *Soil Biol. Biochem.* **1975**, *7* (2), 113−118.
(32) Paynel, F.; Pavlov, A.; Ancelin, G.; Rihouey, C.; Picton, L.; Lebrun, L.; Morvan, C. Polysaccharide Hydrolases Are Released with Mucilages after Water Hydration of Flax Seeds. *Plant Physiol. Biochem.* **2013**, *62*, 54−62.
(33) Naveed, M.; Brown, L. K.; Raffan, A. C.; George, T. S.; Bengough, A. G.; Roose, T.; Sinclair, I.; Koebernick, N.; Cooper, L.; Hallett, P. D. Rhizosphere-Scale Quantification of Hydraulic and Mechanical Properties of Soil Impacted by Root and Seed Exudates. *Vadose Zone J.* **2018**, *17*, 0.
(34) Oleghe, E.; Naveed, M.; Baggs, E. M.; Hallett, P. D. Plant Exudates Improve the Mechanical Conditions for Root Penetration through Compacted Soils. *Plant Soil* **2017**, *421* (1−2), 19.
(35) Sposito, G. Green Water and Global Food Security. *Vadose Zone J.* **2013**, *12* (4), 0.
(36) Bolt, G. H.; De Boodt, M. F.; Hayes, M. H. B.; McBride, M. B. *Interactions at the Soil Colloid- Soil Solution Interface*; Springer, 2015; Vol. *1*, DOI DOI: 10.1017/CBO9781107415324.004.
(37) Ferrage, E.; Sakharov, B. A.; Michot, L. J.; Delville, A.; Bauer, A.; Lanson, B.; Grangeon, S.; Frapper, G.; Jiménez-Ruiz, M.; Cuello, G. J. Hydration Properties and Interlayer Organization of Water and Ions in Synthetic Na-Smectite with Tetrahedral Layer Charge. Part 2. Toward a Precise Coupling between Molecular Simulations and Diffraction Data. *J. Phys. Chem. C* **2011**, *115* (5), 1867−1881.
(38) Dazas, B.; Lanson, B.; Breu, J.; Robert, J. L.; Pelletier, M.; Ferrage, E. Smectite Fluorination and Its Impact on Interlayer Water Content and Structure: A Way to Fine Tune the Hydrophilicity of Clay Surfaces? *Microporous Mesoporous Mater.* **2013**, *181*, 233.
(39) Ferrage, E. Investigation of the Interlayer Organization of Water and Ions in Smectite from the Combined Use of Diffraction Experiments and Molecular Simulations. A Review of Methodology, Applications, and Perspectives. *Clays Clay Miner.* **2016**, *64*, 348.
(40) Tertre, E.; Prêt, D.; Ferrage, E. Influence of the Ionic Strength and Solid/Solution Ratio on Ca(II)-for-Na+ Exchange on Montmorillonite. Part 1: Chemical Measurements, Thermodynamic Modeling and Potential Implications for Trace Elements Geochemistry. *J. Colloid Interface Sci.* **2011**, *353* (1), 248−256.
(41) Ferrage, E.; Lanson, B.; Malikova, N.; Planc, A.; Sakharov, B. A.; Drits, V. A.; En, V.; Group, G.; Ge, M.; Fourier, J. New Insights on the Distribution of Interlayer Water in Bi-Hydrated Smectite from X-Ray Diffraction Profile Modeling of 00 l Reflections. *Chem. Mater.* **2005**, *17* (13), 3499−3512.
(42) Fischer, H.; Meyer, A.; Fischer, K.; Kuzyakov, Y. Carbohydrate and Amino Acid Composition of Dissolved Organic Matter Leached from Soil. *Soil Biol. Biochem.* **2007**, *39* (11), 2926−2935.
(43) Van Hees, P. A. W.; Jones, D. L.; Finlay, R.; Godbold, D. L.; Lundström, U. S. The Carbon We Do Not See - The Impact of Low Molecular Weight Compounds on Carbon Dynamics and Respiration in Forest Soils: A Review. *Soil Biol. Biochem.* **2005**, *37* (1), 1−13.
(44) Hodge, A. The Plastic Plant: Root Responses to Heterogeneous Supplies of Nutrients. *New Phytol.* **2004**, *162* (1), 9−24.
(45) Lievens, B.; Hallsworth, J. E.; Pozo, M. I.; Belgacem, Z. Ben; Stevenson, A.; Willems, K. A.; Jacquemyn, H. Microbiology of Sugar-Rich Environments: Diversity, Ecology and System Constraints. *Environ. Microbiol.* **2015**, *17* (2), 278−298.
(46) Ryan, P. R.; Delhaize, E. Function and Mechanism of Organic Anion Exudation from Plant Roots. *Annu. Rev. Plant Physiol. Plant Mol. Biol.* **2001**, *52*, 527−560.
(47) Veneklaas, E. J.; Stevens, J.; Cawthray, G. R.; Turner, S.; Grigg, A. M.; Lambers, H. Chickpea and White Lupin Rhizosphere Carboxylates Vary with Soil Properties and Enhance Phosphorus Uptake. *Plant Soil* **2003**, *248* (1−2), 187−197.
(48) Safarik, I.; Santruckova, H. Direct Determination of Total Soil Carbohydrate Content. *Plant Soil* **1992**, *143*, 109−114.
(49) Zhang, W.; He, H.; Zhang, X. Determination of Neutral Sugars in Soil by Capillary Gas Chromatography after Derivatization to Aldononitrile Acetates. *Soil Biol. Biochem.* **2007**, *39* (10), 2665−2669.
(50) Hill, P. W.; Farrar, J. F.; Jones, D. L. Decoupling of Microbial Glucose Uptake and Mineralization in Soil. *Soil Biol. Biochem.* **2008**, *40* (3), 616−624.
(51) Parfitt, R. L.; Greenland, D. J. Adsorption of Polysaccharides by Montmorillonite. *Soil Sci. Soc. Am. J.* **1970**, *34*, 862.
(52) Parfitt, R. L. Mechanism of Adsorption of Polymers and Polysaccharides by Montmorillonite. *Doctor of Philosophy Thesis*, University of Adelaide, 1969. pp 1−163.
(53) Abraham, J. Organic Carbon Estimations in Soils: Analytical Protocols and Their Implications. *Rubber Sci.* **2013**, *26* (1), 45−54.
(54) Derrien, D.; Marol, C.; Balabane, M.; Balesdent, J. The Turnover of Carbohydrate Carbon in a Cultivated Soil Estimated by 13C Natural Abundances. *Eur. J. Soil Sci.* **2006**, *57* (4), 547−557.
(55) Barzen-Hanson, K. A.; Wilkes, R. A.; Aristilde, L. Quantitation of Carbohydrate Monomers and Dimers by Liquid Chromatography Coupled with High-Resolution Mass Spectrometry. *Carbohydr. Res.* **2018**, *468* (August), 30−35.
(56) Chenu, C.; Puget, P.; Balesdent, J. Clay-Organic Matter Associations in Soils : Microstructure and Contribution to Soil Physical Stability. *Proc. Unité Sci. du Sol, INRA 78026 Versailles, Fr.* **1993**, No. No. 1, 1−9.
(57) Brax, M.; Buchmann, C.; Schaumann, G. E. Review Article Biohydrogel Induced Soil-Water Interactions: How to Untangle the Gel Effect? A Review. *J. Plant Nutr. Soil Sci.* **2017**, *180*, 121.
(58) Brax, M.; Buchmann, C.; Schaumann, G. E. Effect of Mucilage on Water Properties in the Rhizosphere Monitored By1H-NMR Relaxometry. *Microporous Mesoporous Mater.* **2018**, *269*, 47−50.
(59) Chenu, C.; Pons, C. H.; Robert, M. Interaction of Kaolinite and Montmorillonite with Neutral Polysaccharides. *Proc. Int. Clay Conf. Denver, 1985* **1987**, *381* (January 1987), 375−381.
(60) Carminati, A.; Moradi, A. B.; Vetterlein, D.; Vontobel, P.; Lehmann, E.; Weller, U.; Vogel, H. J.; Oswald, S. E. Dynamics of Soil Water Content in the Rhizosphere. *Plant Soil* **2010**, *332* (1), 163−176.
(61) Brigatti, M. F.; Galán, E.; Theng, B. K. G. Chapter 2 - Structure and Mineralogy of Clay Minerals. In *Developments in Clay Science Vol. 5*; Bergaya, F., Gerhard, L., Eds.; Newnes, 2013; pp 21−81.
(62) Ferrage, E.; Lanson, B.; Sakharov, B. A.; Drits, V. A. Investigation of Smectite Hydration Properties by Modeling

DOI: 10.1021/acs.jpcc.9b09246
J. Phys. Chem. C 2019, 123, 28816−28827

Experimental X-Ray Diffraction Patterns: Part I: Montmorillonite Hydration Properties. *Am. Mineral.* **2005**, *90* (8−9), 1358−1374.
(63) Hatch, C. D.; Wiese, J. S.; Crane, C. C.; Harris, K. J.; Kloss, H. G.; Baltrusaitis, J. Water Adsorption on Clay Minerals as a Function of Relative Humidity: Application of BET and Freundlich Adsorption Models. *Langmuir* **2012**, *28* (3), 1790−1803.
(64) Berend, I.; Cases, J. M.; Francois, M.; Uriot, J. P.; Michot, L. J.; Thomas, F. Mechanism of Adsorption and Desorption of Water Vapor by Homoionic Montmorillonite. *Clays Clay Miner.* **1995**, *43* (3), 324−336.
(65) Ferrage, E.; Lanson, B.; Michot, L. J.; Robert, J. L. Hydration Properties and Interlayer Organization of Water and Ions in Synthetic Na-Smectite with Tetrahedral Layer Charge. Part 1. Results from X-Ray Diffraction Profile Modeling. *J. Phys. Chem. C* **2010**, *114* (10), 4515−4526.
(66) Lindholm, J.; Boily, J.-F.; Holmboe, M. Deconvolution of Smectite Hydration Isotherms. *ACS Earth Sp. Chem.* **2019**, DOI: 10.1021/acsearthspacechem.9b00178.
(67) Aristilde, L.; Galdi, S. M.; Kelch, S. E.; Aoki, T. G. Sugar-Influenced Water Diffusion, Interaction, and Retention in Clay Interlayer Nanopores Probed by Theoretical Simulations and Experimental Spectroscopies. *Adv. Water Resour.* **2017**, *106*, 24−38.
(68) Yeşilbaş, M.; Holmboe, M.; Boily, J. F. Cohesive Vibrational and Structural Depiction of Intercalated Water in Montmorillonite. *ACS Earth Sp. Chem.* **2018**, *2* (1), 38−47.
(69) Mooney, R. W.; Keenan, A. G.; Wood, L. A. Adsorption of Water Vapor by Montmorillonite. I. Heat of Desorption and Application of BET Theory. *J. Am. Chem. Soc.* **1952**, *74* (6), 1367−1371.
(70) Russell, J. D.; Farmer, V. C. Infra-Red Spectroscopic Study of the Dehydration of Montmorillonite and Saponite. *Clay Miner.* **1964**, *5* (32), 443−464.
(71) Madejová, J. FTIR Techniques in Clay Mineral Studies. *Vib. Spectrosc.* **2003**, *31* (1), 1−10.
(72) Yan, L.; Roth, C. B.; Low, P. F. Changes in the Si−O Vibrations of Smectite Layers Accompanying the Sorption of Interlayer Water. *Langmuir* **1996**, *12* (18), 4421−4429.
(73) Rinnert, E.; Carteret, C.; Humbert, B.; Fragneto-Cusani, G.; Ramsay, J. D. F.; Delville, A.; Robert, J. L.; Bihannic, I.; Pelletier, M.; Michot, L. J. Hydration of a Synthetic Clay with Tetrahedral Charges: A Multidisciplinary Experimental and Numerical Study. *J. Phys. Chem. B* **2005**, *109* (49), 23745−23759.
(74) Schellenberger, S.; Drake, H. L.; Kolb, S. Functionally Redundant Cellobiose-Degrading Soil Bacteria Respond Differentially to Oxygen. *Appl. Environ. Microbiol.* **2011**, *77* (17), 6043−6048.
(75) Lynd, L. R.; Weimer, P. J.; van Zyl, W. H.; Pretorius, I. S. Microbial Cellulose Utilization: Fundamentas and Biotechnology. *Microbiol. Mol. Biol. Rev.* **2002**, *66* (3), 506−577.
(76) Clay Mineral Society, Source Clays. http://www.clays.org/sourceclays_history.html (accessed Feb 5, 2016).
(77) Sakharov, B. A.; Naumov, A. S.; Drits, V. A. X-Ray Diffraction by Mixed-Layer Structures with Random Distribution of Stacking Faults. *Dokl. Akad. Nauk SSSR* **1982**, *265*, 339−343.
(78) Hellrup, J.; Holmboe, M.; Nartowski, K. P.; Khimyak, Y. Z.; Mahlin, D. Structure and Mobility of Lactose in Lactose/Sodium Montmorillonite Nanocomposites. *Langmuir* **2016**, *32* (49), 13214.
(79) Lee, S. L.; Debenedetti, P. G.; Errington, J. R. A Computational Study of Hydration, Solution Structure, and Dynamics in Dilute Carbohydrate Solutions. *J. Chem. Phys.* **2005**, *122* (20), 204511.
(80) Ramadugu, S. K.; Chung, Y. H.; Xia, J.; Margulis, C. J. When Sugars Get Wet. A Comprehensive Study of the Behavior of Water on the Surface of Oligosaccharides. *J. Phys. Chem. B* **2009**, *113* (31), 11003−11015.

DOI: 10.1021/acs.jpcc.9b09246
J. Phys. Chem. C 2019, 123, 28816−28827